AIAA Journal
Vol. 43, No. 3, March 2005

Three-Dimensional Planar Doppler Velocity Measurements in a Full-Scale Rotor Wake

Robert L. McKenzie*
MetroLaser, Inc., Sunnyvale, California 94087
and
Michael S. Reinath†
NASA Ames Research Center, Moffett Field, California 94035

The application of planar Doppler velocimetry (PDV) measurements to three-dimensional velocity vector fields in the tip-vortex flows between the blades of a full-scale UH-60 rotor operating in the 80- by 120-Foot Wind Tunnel at NASA Ames Research Center is described. The unique capabilities of PDV for remotely measuring complex velocity fields in large-scale flows are demonstrated and the factors affecting the quality of PDV data from a large-scale facility are defined. Because the wind tunnel is a noncirculating, in-draft configuration, and very large, the principal factor that prevented the acquisition of time-resolved, instantaneous measurements was the spatially and temporally sporadic behavior of the aerosol seeding in the sample area. Nevertheless, time-averaged velocity fields were obtained that characterize the locations and velocity distributions of the blade tip vortices and that provide magnitudes and directions of the velocity vectors in the surrounding flow with better than 1-cm spatial resolution within a square, 1.2 m × 1.2 m, sample area from distances up to 20 m.

Introduction

Objectives

SINCE the inception of planar Doppler velocimetry (PDV), its capabilities have been advanced from simple time-averaged measurements in bench-top jets and small wind tunnels to its present intrinsic capability for instantaneous measurements of complex, three-dimensional, and unsteady flows in large-scale wind tunnels. The fundamental technical development of the concept has reached a state of maturity where the remaining needs for advances pertain mainly to specific applications.

The aim of this paper is to demonstrate the unique capabilities of PDV that enable the remote measurements of complex, three-dimensional, velocity vector fields in large-scale flows at long distances. This has been done to the extent possible within the limited testing opportunities by the application of PDV measurements to the highly dynamic tip-vortex flows between the blades of a full-scale UH-60 rotor operating in the 80- by 120-Foot Wind Tunnel of the National Full-Scale Aerodynamic Complex (NFAC) at NASA Ames Research Center, the world's largest wind tunnel. The measurements reported here represent the second attempt to apply PDV to a rotor in the NFAC and incorporate the refinements realized from the less definitive first attempt.[1] These tests were part of a comprehensive experimental program to explore ways to minimize the strength of the acoustic fields generated by the rotor. The interaction of an advancing blade with the residual blade–tip vortices from one or more previous blades are primarily responsible for the acoustic field generation. Thus far, computational predictions of these complex interactions have not been reliable.

The application of PDV measurements offers a new opportunity to probe quantitatively the aerodynamic structure of the critical flow regions in a more definitive way than has been viable using other experimental techniques in a full-scale experiment. In particular, the application of PDV in this test environment demonstrates its unique capability to provide simultaneous measurements of all three components of the velocity vector magnitudes and directions in an area with dimensions exceeding 1 m, at distances of at least 20 m, and with a spatial resolution of better than 1 cm.

On the other hand, this paper reports only time-averaged measurements of the velocity fields. From previous analytical studies and bench-top experiments,[1–3] PDV technology has been shown to be capable of instantaneous measurements from each laser pulse in large facilities, and such measurements were included in the original objectives of these experiments. However, because the wind tunnel used in these studies is a noncirculating, in-draft configuration and is very large, the spatially and temporally sporadic behavior of the aerosol seeding in the sample area required the PDV fields to be temporally averaged over several hundred laser pulses to accumulate the velocity fields within a significant flow region. Applications in large wind tunnels with recirculating flow, where the aerosol can accumulate in the circuit and fill the test section, should not encounter this limitation.

Background

The concept of PDV was originally named "Doppler global velocimetry" in 1991 by its inventors, Komine et al.[4] Shortly afterward, Meyers,[5] Meyers et al.,[6] and Lee et al.[7] pioneered further developments and performed the first aerodynamic testing applications. Since then, the technique has continued to be developed and has been shown by several laboratories[2,3,8,9] to offer an attractive means for measuring spatially resolved, three-dimensional velocity vectors everywhere in the plane of a laser light sheet in the flow. Because the concept provides planar rather than global field measurements, the more precise name planar Doppler velocimetry[2,9–11] was later adopted. Since then, numerous developments and new applications using both names have been reported.[1,11–18] Detailed descriptions of the PDV concept and its development history may be found in recent review articles by Elliott and Beutner,[18] Samimy and Wernet,[19] and Reinath.[20] In addition, a special publication edited by Elliott[21] describes advances up to the end of the year 2000.

PDV has been demonstrated in low-speed flows, where its accuracy and velocity resolution is restricted mainly by coherent speckle

---

Presented as Paper 2004-2474 at the AIAA 24th Aerodynamic Measurement Technology and Ground Testing Conference, Portland, OR, 28 June–1 July 2004; received 12 July 2004; revision received 22 October 2004; accepted for publication 24 October 2004.

*Senior Scientist, 825 Cathedral Drive; rmckenzie@metrolaserinc.com. Associate Fellow AIAA.

†Aerospace Engineer, Mail Stop N237-7, Advanced Aircraft and Powered Lift Branch.

noise in the images of scattered laser light[3,15] and in sonic and supersonic flows where the Doppler shift is large and where the dynamic frequency range of the optical filter used to discriminate the Doppler shifts must be expanded at the expense of degraded velocity resolution.[9,10] For low-speed measurements, the minimum resolved velocity can be less than 2 m/s (Ref. 3). The use of both continuous-wave and pulsed lasers has been described, but pulsed lasers are particularly attractive because they provide a sequence of instantaneous velocity fields from which determinations can subsequently be made of the pulse-averaged velocities and their statistical or periodic fluctuations. PDV using pulsed lasers has been shown to be especially well suited for applications in large-scale test facilities[2,13] because of the following features:

1) Adequate radiometric signals can be expected at ranges of tens of meters owing to the efficient light scattering by aerosols larger than the wavelength of the laser light.

2) There is no need to resolve and track individual particles or particle gradients in the flow optically to determine their speed.

3) Control of the aerosol seeding density and its distribution in the flow is minimal, requiring only that the aerosol fill the observation area.

4) PDV is not sensitive to small changes in light-sheet position, nor does it require the alignment of multiple beams, thereby minimizing its sensitivity to facility vibrations.

However, many large aerodynamic test facilities operate at low subsonic flow speeds, typically in the range of only tens of meters per second. Moreover, the velocity perturbations relative to the freestream flow that are caused by an aerodynamic body or by turbulence or flow oscillations may be only a few meters per second in some important cases. Thus, the viability of PDV for aerodynamic testing in large facilities was not entirely obvious until its measurement uncertainties were shown to be sufficiently low to resolve the low flow speeds and perturbations that are most prevalent. The results of those studies were originally reported by McKenzie[2,3] and revisited later by others.[9,10,13,15] The outcome encouraged the large-scale applications that followed.[1,12,13,17]

PDV Concept

The PDV concept is based on the illumination of aerosol particles moving in a flow by a sheet of narrowband laser light to obtain filtered images of the Doppler-shifted light scattered from each point in the field of view. The Doppler-shifted frequencies are detected by imaging the scattered light through a sharp-edged spectral filter that transmits or absorbs the light reaching each pixel, in proportion to its Doppler-shifted frequency. The filtered image is then normalized by an unfiltered image of the same view to remove all spatial intensity variations except those associated with frequency shifts. A particularly ideal arrangement for such measurements is the use of molecular iodine vapor as the spectral filter, together with a frequency-narrowed Nd-YAG laser operating at its second-harmonic frequency of 532 nm. The laser is normally tuned to a frequency on the edge of an iodine vapor absorption feature, where the transmission of the unshifted laser light is near 50%. Frequency-narrowed Nd-YAG lasers are easily tuned over a range of wavelengths near 532 nm where the iodine absorption is rich with spectral features. This use of an iodine vapor filter has been shown[2] to provide a spectral resolution that is sufficiently narrow to detect frequency changes of less than 0.5 MHz, which is equivalent to velocity resolutions near 1 m/s, depending on the geometry of the setup.

The characteristics of the absorption spectrum of iodine vapor that are relevant to PDV were originally discussed in detail for a similar filtered Rayleigh velocimetry technique and numerically modeled by Forkey[22] and Forkey et al.[23] The iodine spectral absorption edge used for all of this work was the high-frequency side of the prominent feature at a center frequency of 18,787.81 cm^{-1}, which was labeled by Gerstenkorn and Luc[24] as line 1109.

PDV Measurements in Full-Scale Rotor Wakes

One of the major facilities used for the aerodynamic testing of full-scale rotors has been the 80- by 120-Foot Wind Tunnel of the NFAC at NASA Ames Research Center. The scale of the facility is indicated by the aerial view of the inlet shown in Fig. 1. The structure behind the inlet houses the 80-ft-high by 120-ft-wide test section. The test section then connects to the larger building where the drive fans are located and shared with a closed-circuit 40- by 80-Foot Wind Tunnel. The first application of PDV to interblade flowfields was for a full-scale XV-15 rotor operating in the NFAC.[1] In Ref. 1 a detailed laboratory verification of PDV measurement capabilities on a rotating wheel and in calibrated, low-speed, bench-top flows is also described. However, because that was the first PDV test in the NFAC, the quality of the measurements was compromised by unanticipated, severe optical distortion in the images of one camera, owing to a curved Plexiglas® dome window in the test section side wall. Nevertheless, the initial measurements confirmed the ability of PDV to obtain velocity fields at the distances imposed by the facility and made evident the instrumental issues that needed further refinement.

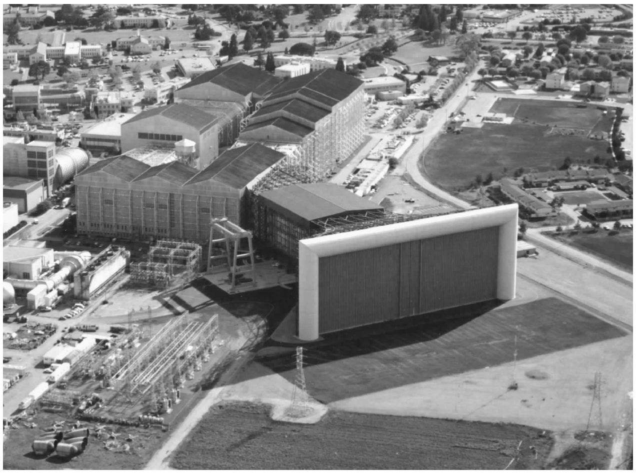

Fig. 1 Inlet of the 80- by 120-Foot Wind Tunnel at the NASA Ames Research Center NFAC.

Experimental Setup

UH-60 Test Model

In the experiments reported in this paper, the test model was the UH-60 rotor mounted on the large rotor test apparatus (LRTA) shown in Fig. 2. The scale of the installation is characterized by the height of the rotor hub, which was 12 m (39 ft) above the test section floor. The rotor assembly included four blades, each with a radius of 817 cm, a chord of 52 cm, and a 58-cm tip section that was skewed backward with a 19-deg sweep. The direction of rotation was counterclockwise when viewed from above so that the blade advancing into the flow was on the starboard (right) side of the model in Fig. 2.

PDV Geometry

The fundamental geometry for PDV measurements is illustrated by the vectors shown in the light sheet in Fig. 3. The frequency of the scattered laser light is Doppler shifted in proportion to the component of aerosol speed in the direction of the velocity component that is observed by each camera. The primary geometrical parameters are the unit vectors $\boldsymbol{l}$ and $\boldsymbol{a}$, which denote the directions of the light sheet propagation and the observer, respectively, as shown in Fig. 3. The direction and scale factor of the associated velocity component is then determined by the difference vector, $\boldsymbol{S} = \boldsymbol{a} - \boldsymbol{l}$. By measurement of the Doppler frequency shifts at each point in the light sheet that is commonly observed by all three cameras, from three different directions, the resulting nonorthogonal velocity components can be combined to give three orthogonal components that traditionally describe the direction and magnitude of the flow velocity vector at each point.

Fig. 2 Downstream view of the UH-60 rotor mounted on the LRTA in the 80- by 120-Foot Wind Tunnel at the NFAC at NASA Ames Research Center.

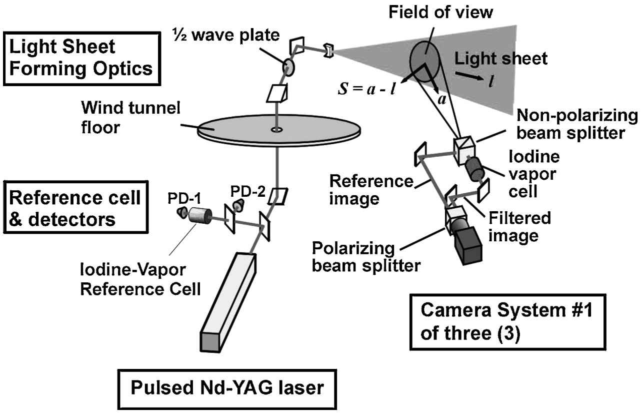

Fig. 3 Schematic of PDV optical system.

PDV Optics

The major PDV optical subsystems are shown schematically in Fig. 3, but with only one of three identical camera systems included in Fig. 3. Their functions were as follows.

Pulsed Nd-YAG laser. For the NFAC wind-tunnel installation, the laser and reference cell subsystem were mounted on an optical table located on the mezzanine floor below the test section. The pulsed Nd-YAG laser was capable of generating pulse energies greater than 300 mJ at its frequency-doubled wavelength of 532 nm. The laser was forced to a narrowband, single-axial mode by injection seeding from a diode-pumped, single-mode, Nd-YAG crystal. Frequency locking was achieved using a Q-switch buildup scheme that matched the resonant frequency of the host laser cavity to the seed laser frequency by adjusting the host cavity length. The resulting frequency doubled output was tunable over a range of 2 GHz with a bandwidth of 140 MHz.

However, frequency locking using Q-switch buildup control is known to be extremely sensitive to cavity length disturbances caused by external mechanical vibrations. In this application, the operating rotor was the predominant source of mechanical vibrations, which were sufficiently large to be felt in the feet of someone standing on the concrete floor of the mezzanine where the laser was located. Even with the laser on a vibrationally isolated table, it would not reliably lock to a single axial mode while free running at 10 Hz when the rotor was at its highest speeds and thrust coefficients. Fortunately, when the laser pulses were synchronized to a harmonic of the rotor rotation at approximately 8 Hz, so that the laser pulses were in phase with the periodic rotor disturbances, the laser functioned on a single axial mode without difficulty at all conditions.

Reference cell and detectors. Q-switch buildup control of the laser injection seeding requires about a 10-MHz modulation of the laser frequency from pulse to pulse to seek the minimum buildup time. Consequently, the unshifted laser frequency must be measured together with the frequency of the scattered light from pulse to pulse to measure the small Doppler frequency shifts with sufficient accuracy. To do so, a sample of the laser beam was directed into the reference cell and detectors subsystem as shown in Fig. 3. There, the sampled laser light energy was split so that approximately 50% passed through a cell containing iodine vapor, whereas the remainder bypassed the cell. The pulse waveforms of the two beams were then detected by the photodiodes, PD-1 and PD-2, which observed filtered and unfiltered light, respectively. The temporal integrals of the filtered and unfiltered waveforms are proportional to the relative pulse energies on each detector. They were obtained with a gated boxcar integrator system and recorded and ratioed by a computer. The ratio of filtered to unfiltered pulse energies enabled the filter transmission and the corresponding laser frequency to be determined for each laser pulse. In addition, a real-time display of the filtered pulse energy facilitated the initial tuning of the laser frequency to 50% transmission on a selected spectral feature of the iodine vapor.

Light-sheet-forming optics. To generate the light sheet, the unexpanded laser beam was directed vertically from the laser optical bench to a housing on the test-section floor that contained the light-sheet-forming optics. There the beam was formed into a fan-shaped light sheet by a train of optical elements including the following: 1) a half-wave plate to rotate the beam polarization, align it with the plane of the light sheet perpendicular to the propagation axis, and thereby maximize the scattered light seen by the cameras; 2) a cylindrical lens that could be rotated about the optical axis to align the plane of the light sheet in the vertical direction and expanded it in one direction; and 3) a polarization-insensitive, 90-deg prism that turned and directed the light-sheet fan upward into a plane that lies parallel to the leading or trailing edge of a rotor blade for a blade azimuth of 90 deg. (Azimuth angle is measured from the horizontal axis pointing downstream and increases counterclockwise when looking down on the rotor.)

Camera systems. For each laser pulse, Doppler-shifted frequencies everywhere in the field of view of the light sheet were recorded simultaneously by each of three separate camera systems. Processed images with gray scales modified by the Doppler-shifted frequencies were obtained by splitting the field of view seen by each camera into two adjacent zones on the image plane, one with its image passing through a cell containing iodine vapor and the other bypassing the cell. Subsequent post-processing divided the filtered image by the unfiltered image to normalize the variations in gray scale not related to Doppler frequency shifts. The numerical technique for filtering and ratioing images pixel by pixel is described in Refs. 1–3. Figure 3 includes a schematic of the slit-image optics for a single camera and Fig. 4 is a photograph of the assembly packaged for harsh wind-tunnel environments.

Test-Section Installations

Figure 5 shows the PDV installation in the NFAC 80- by 120-Foot Wind Tunnel test section, showing the LRTA, the locations of the PDV components, and the optical path lengths from each camera to the sample area. The colored path lengths correspond to similarly colored arrows labeled V_A, V_B, and V_C, that indicate the velocity component directions measured by cameras A, B, and C, respectively. Figure 5 also shows the positions of cameras A and B on the test-section floor in plywood housings. Camera C was located behind a permanent camera port window on the sidewall at a height of 2.2 m above the rotor plane.

The sample area size was determined by the size and location of a mapping target. The mapping target contained a matrix of backlighted holes that enabled the individual pixel locations in each camera to be related to their respective split-image partners and to the common locations in the sample area seen by each of the three cameras. This mapping was necessary to facilitate the normalization of each filtered image by its unfiltered counterpart and then to correlate spatially the vector components from all image points of the three cameras into a single, three-component vector field.

The angles of the camera fields of view were limited to approximately 0.1 rad by the entrance aperature of the image-splitting optics. Thus, the maximum visable diagonal of the square mapping target at the 20-m camera range was 2 m. The target was made from a 143 by 143 cm square by 0.32 cm thick aluminum plate. The 0.9-cm-diam backlighted holes were sized to illuminate just a single pixel, and one side was covered with translucent vellum to diffuse the light illuminating the holes from either side. Figure 6 is a photograph of the target suspended in position for the rotor tests, with its center 85 cm above the rotor plane and 41 cm inboard of the rotor tip location.

Data Acquisition/Control System

The data acquisition/control system used a separate personal computer processor for each camera. The three processors shared a single keyboard, monitor, and mouse using a manual keyboard-video-mouse switch. A fourth computer recorded and displayed the reference cell transmission signals and controlled the laser frequency through an Institute of Electrical and Electronics Engineers 488 input/output interface. The laser was triggered synchronously with the rotor by signals from an encoder on the rotor shaft. Pulses from the encoder pulse train were electronically selected to provide trigger pulse repetition rates within the 8–12-Hz range accepted by the pulse-forming network for the laser flash lamps. An adjustable delay between an encoder synchronizing pulse and the laser trigger

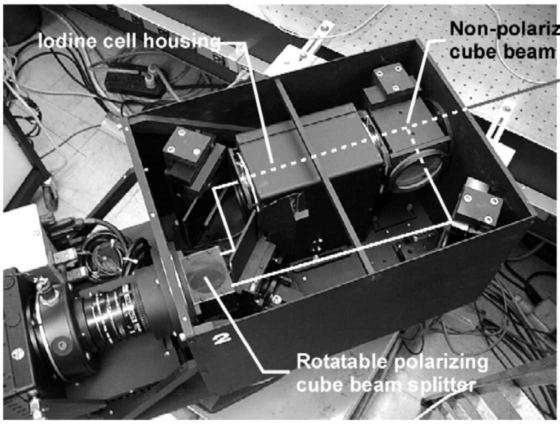

Fig. 4 Split-image camera assembly with housing cover removed.

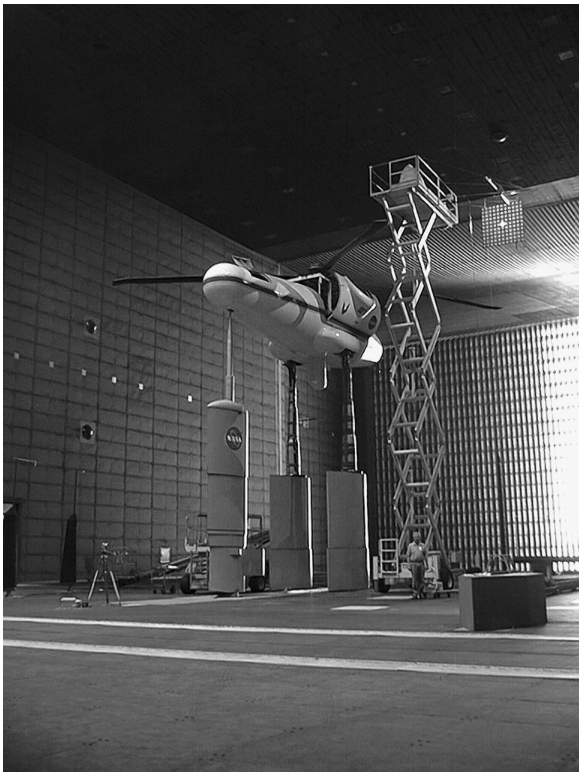

Fig. 6 Backlighted mapping target elevated to its position for rotor tests with its center at 12.8 m above test-section floor and in field of view of all three cameras.

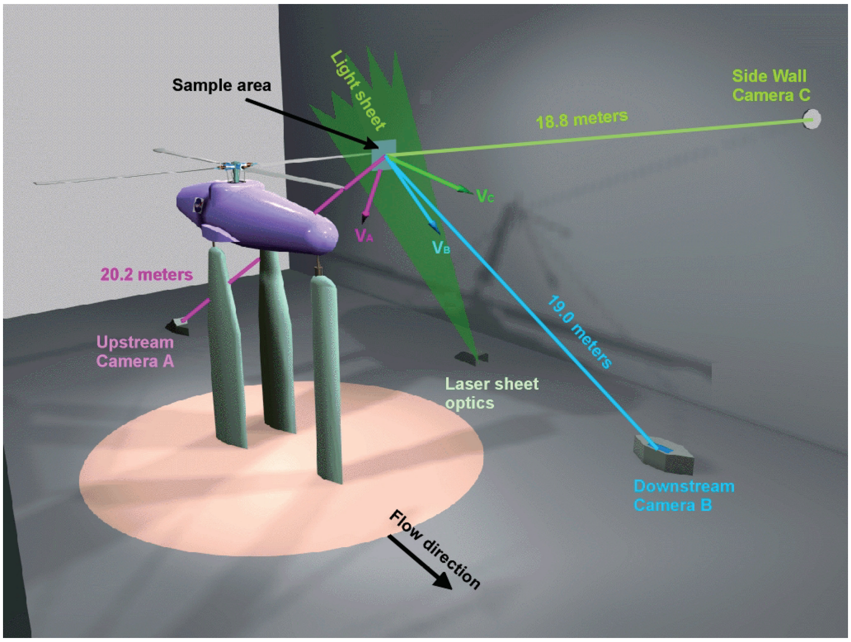

Fig. 5 Schematic of PDV installation in NFAC 80- by 120-Foot Wind Tunnel test section for UH-60/LRTA testing; colored arrows labeled V_A, V_B, and V_C indicate velocity component directions measured by similarly colored cameras A, B, and C, respectively.

enabled the rotor blade position at the time of the laser trigger to be adjusted relative to the light sheet within a few millimeters. For this UH-60 application, where the rotor speed was nominally 258 rpm (4.3 revolutions/s), two encoder pulses per revolution were selected, thereby sending trigger signals to the laser at a repetition rate of 8.6 Hz. However, to accommodate the maximum camera framing rate of 1.9 Hz, image data were acquired only on every seventh laser pulse. As a result, the flowfield velocities were always measured behind the same blade.

Flow Seeding Systems

The uniform seeding of aerosols in the PDV sample area is particularly difficult in a facility the size of the NFAC 80- by 120-Foot Wind Tunnel. In addition, the facility has an in-draft inlet configuration that does not provide recirculation of the seeded flow. Thus, flow seeding was confined to a single pass through the relatively small sample area in the laser light sheet. The most practical means of introducing the aerosols into the flow with minimum disturbance to the flow uniformity in the test section was to locate the smoke generator outside the inlet vanes. However, initial experience from an earlier setup[1] showed that smoke passing through the vanes is entrained by their wakes, mixed with unseeded air, and broken into eddies that separate in the streamwise direction before reaching the sample area. In an effort to fill the vane wakes with only seeded air, an extended version of a smoke generator was constructed with a dispersal array that spanned six vanes and produced a smoke plume that was uniform across the intervane passages.

Several views of the extended seeding system in front of the inlet are shown in Figs. 7a–7e. The system included five, high-volume, commercial smoke units that efficiently converted mineral oil into an aerosol with very small droplet sizes that remain suspended in air for extended periods. Moreover, the mineral oil did not deposit noticeably on surfaces, it had no perceptable odor, and it was neither toxic nor environmentally hazardous.

Each smoke unit independently filled one of the five dispersal tubes in the array. The tubes were 75 mm in diameter by 14.3 m long and spaced horizontally 51 cm apart (Fig. 7a). Each tube contained 13-mm-diam vent holes spaced 30.5 cm apart, in longitudinal rows along their top and bottom surfaces and at each end (Fig. 7b). The size of this arrangement was designed to fill the PDV sample area defined by the mapping target and took into account the contraction ratio of the test-section inlet. The outlets of each smoke unit were vented to draw in cool, ambient air that condensed the heated mineral oil vapor into an aerosol before it entered the dispersal tubes. An inline blower in each hose between each tube and its smoke unit outlet forced the aerosol into the dispersion tubes and out the vent holes. To improve the uniformity of the aerosol distribution, strips of 3-in.-wide webbing were added to the spaces between the tubes to provide a mesh with an open area of 60% (Fig. 7b). The mesh was designed to generate a turbulent wake in the smoke plume with eddy sizes matching the scale of the tube diameter. The entire assembly was mounted on the personnel basket of a man lift (Fig. 7d) that was capable of reaching the inlet centerline 70 ft above the ground and could be moved as needed to adjust the position of the plume while the wind tunnel was running.

Figure 7e also shows that, despite the large size of the dispersal array, it was still very small compared to the wind-tunnel inlet dimensions. Consequently, the smoke plume at the sample area was also small compared to the test-section cross section and was easily deviated from its intended path by small crosswind disturbances. Before the wind-tunnel tests, the smoke system was found to perform well in ambient air with light winds, as shown in Fig. 7c. However, in the wind-tunnel flow, the plume broke into separated eddies in the streamwise direction that created very intermittent seeding in the sample area. Moreover, when the blade lift (thrust coefficient) was high, the centrifugal motion of the blade tip vortices intermittently reduced or eliminated the local aerosols near the vortex core. Thus, whereas single-pulse PDV measurements could be obtained

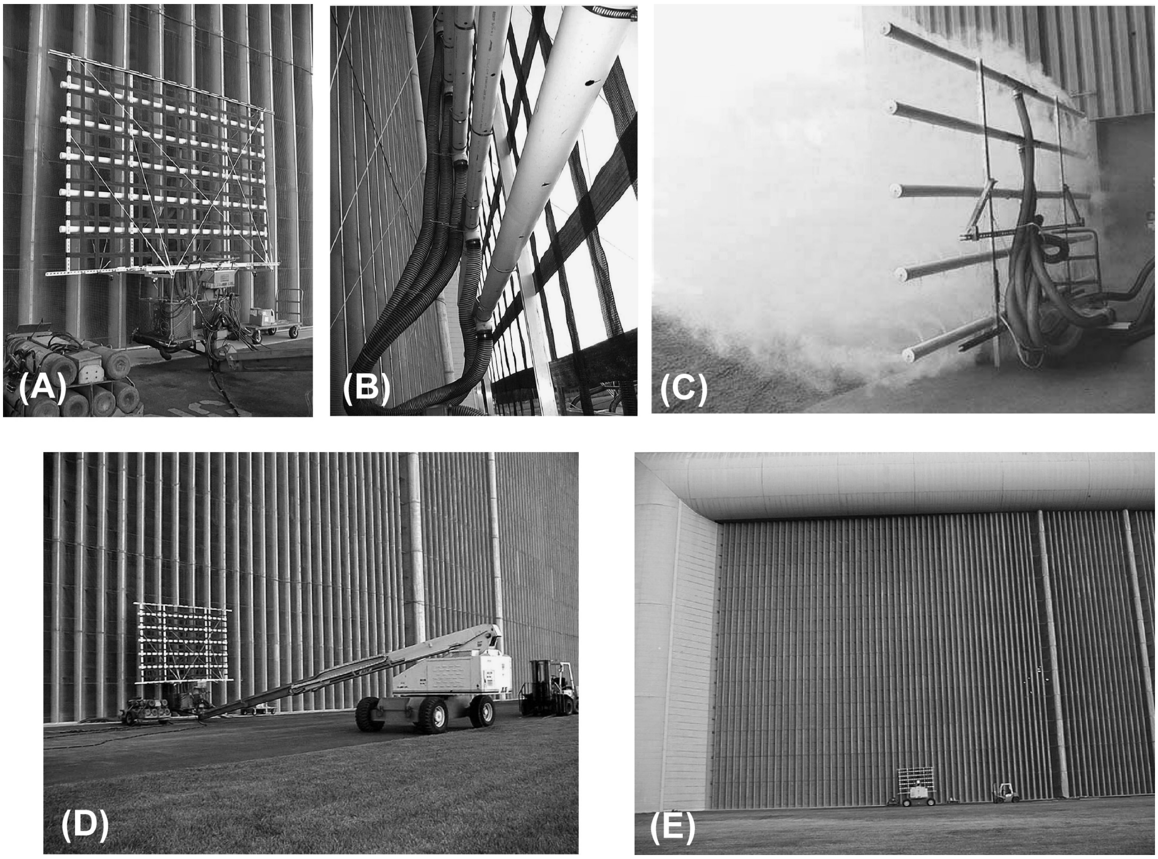

Fig. 7 Extended smoke generator: a) and d) generator assembly mounted in personnel basket of a man lift, b) close-up of smoke tubes, showing vent holes and turbulence-generating webbing, c) assembly in operation with smoke carried away by light wind, and e) size of smoke generator assembly relative to 130-ft-high wind-tunnel inlet.

for a few selected frames, they were too few in number. More generally, the seeding in most individual frames appeared only in isolated or broken regions that were small compared to the total sample area. Nevertheless, by accumulating images over several hundred frames, average measurements over a substantial part of the sample area were accumulated. The averages were computed for each pixel in the sample area by summing and averaging only the signals above a prescribed threshhold. Thus, the number of frames contributing the average is different for each pixel.

Hence, adequate aerosol seeding of the flow in a large, in-draft wind tunnel remains a critical issue for further development. On the other hand, the performance of this type of smoke generator system is expected to be very adequate for applications to most closed-circuit wind-tunnel configurations where the smoke content remains airborne and is recirculated.

Spatial Frequency Gradients in the Light Sheet

Some injection-seeded Nd-YAG lasers have been found to display transverse variations in frequency across their beam cross section even though the frequency at any location remains narrowband. Forkey[22] and Forkey et al.[23] measured radial variations as large as 100 MHz from the beam center to its outer radius. When the laser beam is expanded into a light sheet, the frequency may be expected to vary in the direction normal to its propagation, with the largest gradients near the edges of the sheet. Clancy and Samimy[9] reported spatial frequency variations of 21 MHz in the light sheet from their laser, but were also able to reduce them to 10 MHz by realignment of the seed laser with the host laser. We have observed similar variations in two different lasers, whereas others did not detect the effect.[13]

Unless the spatial frequency variations can be made insignificant, the measured Doppler shift fields must be corrected for them. A solution applied by Clancy and Samimy[9] was to block the light-sheet edges and use only the central region where the frequency gradients were smallest. In our work, we did the same, but also incorporated image corrections using zero-velocity images of the entire light sheet as seen by each camera. To obtain these images, including the same polarization effects created by aerosol scattering in the flow, we were forced to use stationary or slowly moving aerosol in the test section as the target. The zero-velocity field measurements were made the same way as in the wind-tunnel flow. Spatial frequency variations as large as 50 MHz were found and were most pronounced at the edges of the light sheet, as expected.

To correct the Doppler shift fields obtained from the moving aerosols for the spatial frequency gradients, the filter response function was assumed to be nearly linear in its midfrequency region so that, to lowest order, the zero-velocity frequency fields could be simply subtracted from the Doppler-shifted fields obtained with wind-tunnel flow. We believe that this lowest-order correction is adequate for most cases where the Doppler-shifted frequencies do not fall in the highly nonlinear wings of the response function, but the use of a higher-order correction process that accounts for the nonlinear response function would have been preferable.

We also have evidence that the spatial distributions of frequency in the laser light sheet are not constant from pulse to pulse, so that corrections based on time-averaged distributions still contain errors for any single-pulse measurements. This effect is particulary pronounced when the edge of the light sheet is in view, as subsequent results will show. However, in this application, all of our results are also time averaged, which tends to minimize the correction errors owing to temporal variations in the spatial distributions of laser frequency.

Freestream Velocity Field Measurements

PDV measurements were first made during the "aerotare" phase of the UH-60 test program in which the test section contained only the LRTA with its rotors removed. These tests allowed us to characterize the accuracy of the PDV measurements in a relatively steady and uniform flow. However, the uniformity and steadiness of the flow was not fully assured because the original flow-monitoring instruments in the test section were calibrated with an empty test section, whereas in this case the test section contained the LRTA body and a large aeroacoustic microphone rake located on the test-section floor upstream of and below the PDV sample area. The only other independent flow measurement was done with a single pitot probe located upstream and on the opposite side of the LRTA. It provided the values of the freestream reference speed V_{ref}, which may not accurately represent the flow speed everywhere in the test section owing to the disturbances created by the objects in the flow.

Velocity vector fields were measured at freestream speeds of $V_{\mathrm{ref}} = 30$, 60, and 80 kn. An example of the results at 80 kn is shown in Fig. 8. A complete report of all of the PDV measurements is also available.[25] The orthogonal axis set in Fig. 8 and subsequently has the origin of the Y axis at the rotor hub, and it increases in the direction toward the sample area. The X axis points downstream in the streamwise direction, and the Z axis points vertically upward with its origin at the plane of the rotor. The green boxes shown mark an outline of the mapping target boundaries that define the PDV field of view. However, the measured flowfield does not extend over the entire field of view because of the intermittent smoke seeding. Consequently, only regions of the velocity fields are shown that could be temporally averaged over 400 frames. The color contours in Fig. 8a represent values of $V_{\mathrm{tot}}/V_{\mathrm{ref}}$, where V_{tot} is the average total velocity vector magnitude determined from its three measured components. The quality of the PDV measurements is indicated by the measured velocity vector field, which is shown to be generally uniform and in the downstream direction. The spatially averaged total velocity of 76.7 kn ($V_{\mathrm{tot}}/V_{\mathrm{ref}} = 0.96$) indicates the PDV measurement accuracy.

Figure 8b is an edge-on view of the velocity vectors looking along the Y axis outward from the rotor hub. The flow vectors are generally aligned in the downstream direction but indicate some disturbances

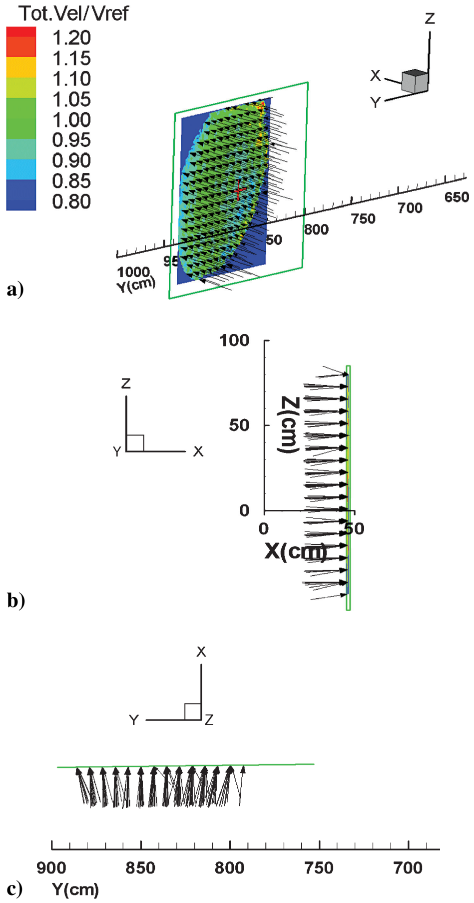

Fig. 8 Aerotare velocity vector field and $V_{\mathrm{tot}}/V_{\mathrm{ref}}$ contours for $V_{\mathrm{ref}} = 80$ kn, field-averaged $V_{\mathrm{tot}}/V_{\mathrm{ref}} = 0.96$ ($V_{\mathrm{tot}} = 76.7$ kn): a) isometric view of the three-dimensional vector field and $V_{\mathrm{tot}}/V_{\mathrm{ref}}$ contours, b) edge view along the Y axis outward from the rotor hub, and c) edge view downward along the Z axis.

at the edges that may be the result of uncorrected frequency gradients in the light sheet. Similarly, a downward view of the vectors, shown in Fig. 8c, indicates some small outflow away from the target center that is most likely a measurement artifact. At lower speeds, consistent inflows toward the hub are seen. These speed-dependent flow directions at the lower speeds suggest that they contain real flow features caused by the LRTA body.

Overall, these aerotare results show that the PDV measurements provide flowfield definitions with sufficient accuracy to characterize the flowfield velocities and their gradients, and they do so for test conditions and measurement ranges where few other remote techniques can simultaneously interrogate as large an area. Finally, although the influence on these results by the tunnel behavior at low speeds and with large objects in the flow cannot be entirely separated from the effects of possible PDV measurement artifacts, the PDV results provide reasonable evidence that some low-speed flow disturbances were present.

Rotor Velocity Field Measurements

PDV measurements were made during the rotor performance phase of the UH-60 tests to characterize the interblade wake fields, with particular attention given to the behavior of the rotor tip vortices. Although our primary purpose in this paper is not to describe rotor flows in detail, the complex, three-dimensional features of the flow serve to demonstrate the unique capabilities of PDV under particularly challenging circumstances. Hence, the results are described in the necessary detail hereafter.

The location of the velocity field measurements is established by the plane of the mapping target, which was aligned with the rotor hub on the 90-deg azimuth. The target center was located 86 cm above the rotor plane with its outboard edge 31 cm beyond the rotor tip. In earlier studies,[1] this area was found to encompass the major features of the tip wakes, including their primary vortices. The laser light sheet was then aligned in the same plane and positioned to cover the sample area.

Because rotor wake measurements were obtained at a sample area location different from that of the aerotare measurements, they were preceded by the repositioning of the mapping target and a realignment of the light sheet and camera fields of view. Unfortunately, we discovered only after the wind-tunnel test was restarted and seeding added to the flow that the laser sheet did not fill the entire sample area defined by the mapping target. Because the expense of delaying the rotor test prevented us from stopping the tunnel flow to reposition the light sheet, the area of the mapping target was not fully illuminated by the light sheet for these wake measurements, and one edge of the light sheet with its undercorrected frequency gradients was in the field of view. However, the locations of those regions are obvious in the field velocity contour images and can be ignored.

All velocity field measurements were made behind the trailing edge of the advancing blade. The rotor plane was at 0-deg angle of attack and rotation speeds were 259±1 rpm. The wind-tunnel airspeed was adjusted to maintain a constant advance ratio of 0.15, resulting in a nominal freestream speed of $V_{\text{ref}} = 64.4 \pm 0.1$ kn. Blade pitch angles were varied to obtain thrust coefficients of $C_T = 0.06$, 0.08, and 0.10. At each value of C_T, we measured relative blade positions and flowfield velocities for blade azimuth angles upstream from the PDV sample area of 15, 30, 45, 60, and 75 deg. A representative sampling of the results is described hereafter. A complete report of the results is given in Ref. 25.

Effects of Thrust on Blade Position

An associated benefit of the PDV instrumentation was its ability to obtain photogrammetric measurements of dynamic blade positions as they vary with thrust loads. Furthermore, we must know the vertical position of the blade tip where it passes through the sample area to characterize the interblade wake geometry. The 817-cm-long blades are flexible in bending, and they had pivoting attachments at the hub that allowed the blade azimuth angle to lead or lag freely the rotor hub azimuth. Thus, both motions had an uncontrolled dependence on the thrust coefficient. However, they could be determined for any condition by measuring the locations of the blade tips in the light sheet using the PDV instrumentation.

Blade lead-lag. The blade angular position relative to the laser light sheet could be adjusted within the width of the laser light sheet by manually varying the delay between the encoder output at zero rotor azimuth and the laser trigger. A tip delay for each C_T was determined by finding the trigger delay where the trailing edge of the blade tip was just inside the light sheet. From the camera images, the uncertainty of the blade tip penetration into the light sheet appeared to be less than ±2 cm, which is equivalent to an uncertainty in the relative blade rotational position of less than ±0.2 deg.

The variations in tip delay with C_T are an indication of the blade lead-lag behavior. As C_T was increased, the delay time for the blade to arrive at the 90-deg azimuth increased, which was interpreted as an increase in lag angle. Moreover, the difference in delay times between the arrival of the blade leading edge and its trailing-edge exit remained constant for all C_T, which corroborated the interpretation of the delay measurements. The results of the delay measurements are shown in Fig. 9a as lag angles measured relative to the blade position when $C_T = 0.02$. The lower three points vary nearly linearly with C_T, and the exceptional point at $C_T = 0.10$ is validated by its repeatability.

Blade height. The effect of C_T on blade height was measured by noting the pixel coordinates of the blade tip in the images from each PDV camera as it passed through the light sheet. The mapping target analysis then enabled a determination of the physical blade tip height from any of the three camera images. The side-wall camera C gave the least uncertainty because it was only 2.2 m above the blade plane. The results are shown in Fig. 9b in terms of effective blade dihedral (or cone) angles. They vary linearly with C_T for all values.

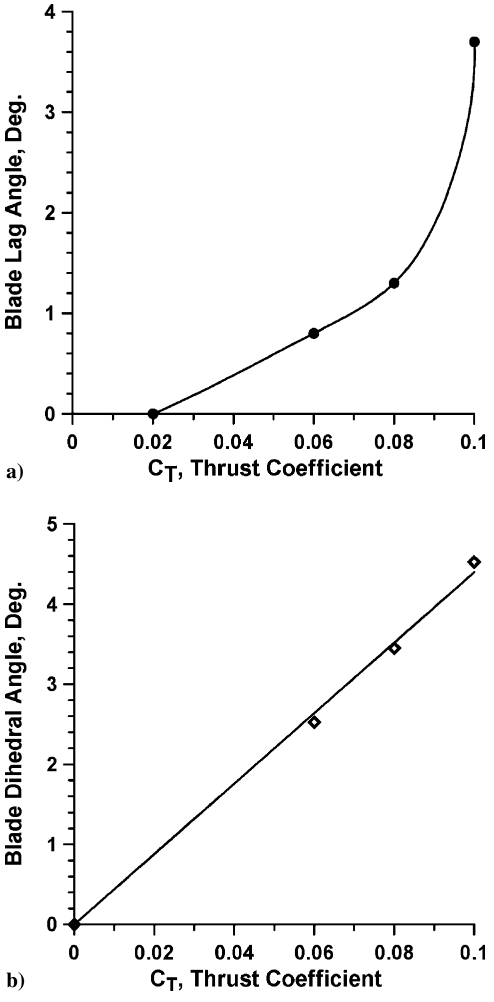

Fig. 9 Effect of thrust coefficient on rotor blade: a) lag angle and b) dihedral angle.

These results are represented in the subsequent velocity field images as red crosses that mark the Y, Z coordinates where the blade tip passes through the light sheet for the corresponding thrust.

Blade Wake Measurements

In the following field plots shown in Figs. 10–13, the orthogonal velocity components in the blade wakes are represented by U, V, and W, where U is the axial component in the downstream direction of the X axis, V is the transverse component along the Y axis in the direction outward from the rotor hub, and W is the vertical component upward along the Z axis. The freestream airspeed is denoted by V_{ref} and is used as the normalizing factor for all of the nondimensional velocity component values presented.

The spatial resolution of PDV field measurements is limited by the pixel size of the charge-coupled device array and the camera lens magnification. For these tests, the spatial resolution of each pixel was 0.7 cm. The PDV image processing incorporated spatial averaging over a sliding 3 × 3 pixel area in the image plane, but the results still reveal sharp features smaller than 1 cm. This capability is particularly evident in images of the mapping target where 0.9-cm-diam backlighted holes illuminate a single pixel, producing a predominate peak signal with only much weaker signals in the adjacent pixels. In most cases, the three-pixel averaging process spreads the image to one additional pixel in each image-plane direction but still retains the central peak position.

Effects of wake age. The effects of wake age, which are represented by an increase in the blade azimuth angle relative to the light sheet, were revealed by comparing velocity fields at a fixed thrust coefficient, $C_T = 0.08$, for blade trailing-edge azimuth angles of 15, 30, 45, 60, and 75 deg upstream of the light-sheet plane. At this thrust, the presence of an isolated primary vortex from the blade tip can be identified by its highly localized and mostly symmetrical distribution of axial (streamwise) velocity components. Examples for the blade azimuths of 15 and 60 deg are shown in Figs. 10 and 11. In both cases, the freestream airspeed is $V_{\mathrm{ref}} = 64.3$ kn and the nominal rotor speed is 259.6 rpm. Figures 10a and 11a show the axial velocity field, U/V_{ref}, looking along the X axis in the downstream direction.

The green square marks the outline of the mapping target area and the red cross marks the passage point of the blade tip through the sample area plane. The the primary vortex core center may be identified in Figs.10a and 11a by a localized red dot located above and inboard of the blade tip passage point. As blade azimuth increases, the core position moves higher and farther inboard. Figures 10b and 11b show distributions through the vortex core center of axial velocity increments $(U - V_{\mathrm{ref}})/V_{\mathrm{ref}}$ and vertical velocities W/V_{ref}. At the blade azimuth of 15 deg, the velocity distributions in Fig. 10b indicate a well-defined vortex behind the blade trailing edge with a core diameter of approximately 8 cm. In addition, a weaker secondary vortex appears as a localized red dot that is higher and farther inboard near $Y, Z = (778, 85)$, most likely trailing from the previous blade.

Figure 11 shows the axial velocity field when the blade has moved farther upstream to an azimuth of 60 deg. In this case, the blade causing the disturbance has passed out of sight upstream, and the next approaching blade can be seen as it advances from the rear, downstream of the sample plane. Now the primary tip vortex has become more broadly distributed and appears to have separated into two interacting vortices.

Effects of thrust coefficient. The effects of thrust coefficient on the wake velocity fields were measured for $C_T = 0.06$, 0.08, and 0.10. In all cases, the blade azimuth was 15 deg. Figures 12 and 13 show examples for $C_T = 0.06$ and 0.10, respectively. For both cases, the freestream airspeed was $V_{\mathrm{ref}} = 64.5$ kn, and the nominal rotor speed was 258.0 rpm. Figures 12a and 13a show the axial velocity fields, U/V_{ref}, and Figs. 12b and 13b show the projection of the velocity vectors on the plane of the light sheet. Figures 12c and 13c

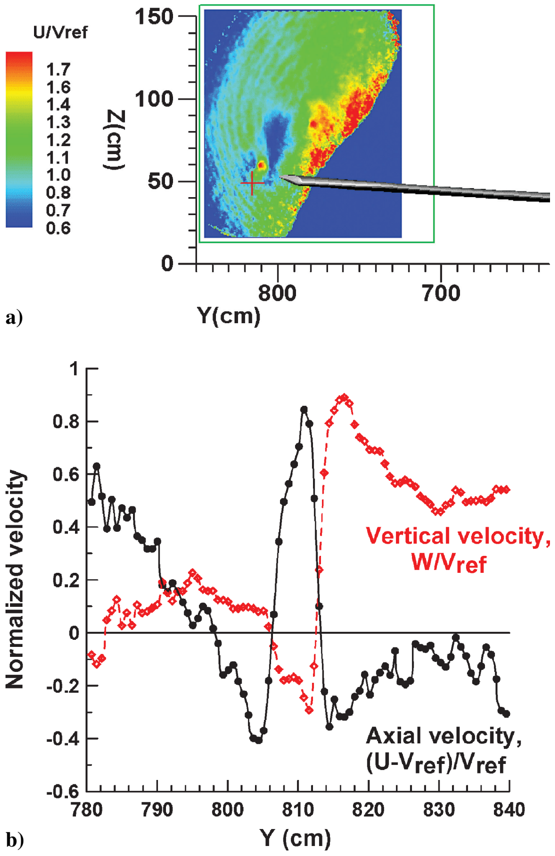

Fig. 10 Blade-wake velocity fields: normalized axial a) velocity field contours (U/V_{ref}) for blade trailing-edge azimuth of 15 deg upstream of light sheet, primary tip vortex core center in upper right quadrant of cross at $Y, Z = (810.9, 60.0)$ and b) $[(U - V_{\mathrm{ref}})/V_{\mathrm{ref}}]$ and vertical $[W/V_{\mathrm{ref}}]$ velocity profiles through the primary tip vortex core at constant $Z = 60.0$ cm, plotted along a line parallel to the Y axis.

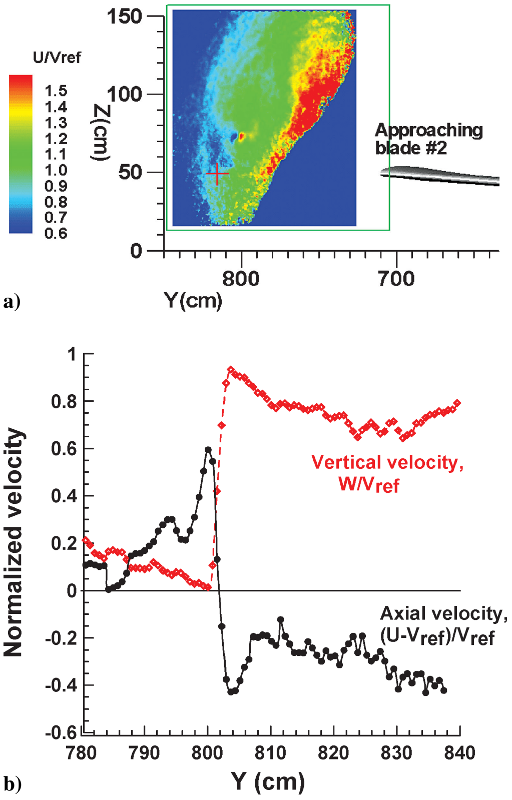

Fig. 11 Blade-wake velocity fields: normalized axial a) velocity field contours (U/V_{ref}) for blade trailing-edge azimuth of 60 deg upstream of the light sheet, primary tip vortex core center in upper right quadrant of red cross at $Y, Z = (800.1, 73.6)$ and b) $[(U - V_{\mathrm{ref}})/V_{\mathrm{ref}}]$ and vertical $[W/V_{\mathrm{ref}}]$ velocity profiles through the primary tip vortex core at constant $Z = 73.6$ cm.

show the velocity vector profile along a vertical strip at $Y = 800$ cm, looking along the Y axis toward the rotor hub, and Figs. 12d and 13d show the velocity vector profile along a horizontal strip at $Z = 107$ cm, looking downward.

The axial velocity contours in Figs. 12a, where the aerodynamic lift is smallest, show no significant velocity field disturbances that clearly indicate a rotor tip vortex. The missing vortex is explained by the circulating velocity vectors shown in Fig. 12b, which suggest that the primary tip vortex core center is below the data area, near Y, $Z = (816, 40)$ and is not fully located in the sample area. Figure 12b also indicates a general flow above the blade in the inboard direction. That behavior is corroborated in the downward view of Fig. 12d. Finally, Fig. 12c indicates that the flow above the blade has no significant vertical component in the vertical strip sampled.

The results are shown in Figs. 13 for increased aerodynamic lift at $C_T = 0.10$. In this case, the centrifugal strength of the primary vortex was sufficient to fling most aerosols from the vortex core for all 400 frames averaged, as seen by the curled void in Figs. 13a and 13b and in the circulation about it as shown in the vector field in Fig. 13b. No clear indication of a primary tip vortex core center is apparent in the data area, except perhaps from the centroid of the seeding void where the aerosol has been flung out of the core, but an expanded view of Fig. 13a would show a cluster of three vorticies centered at Y, $Z = (811, 71)$. The velocity vectors surrounding the void also corroborate the presence of a vortex at the center of the void. Another broadly dispersed circulation area is indicated by the green region in Fig. 13a centered at Y, $Z = (790, 105)$, which may be caused by the previous blade. Regardless of the disorganized velocity fields measured at this thrust, they show that the field structures are different from those at lower thrust. On the other hand, the vector profiles sampled in the vertical and horizontal directions in Figs. 13c and 13d, respectively, do not appear significantly different.

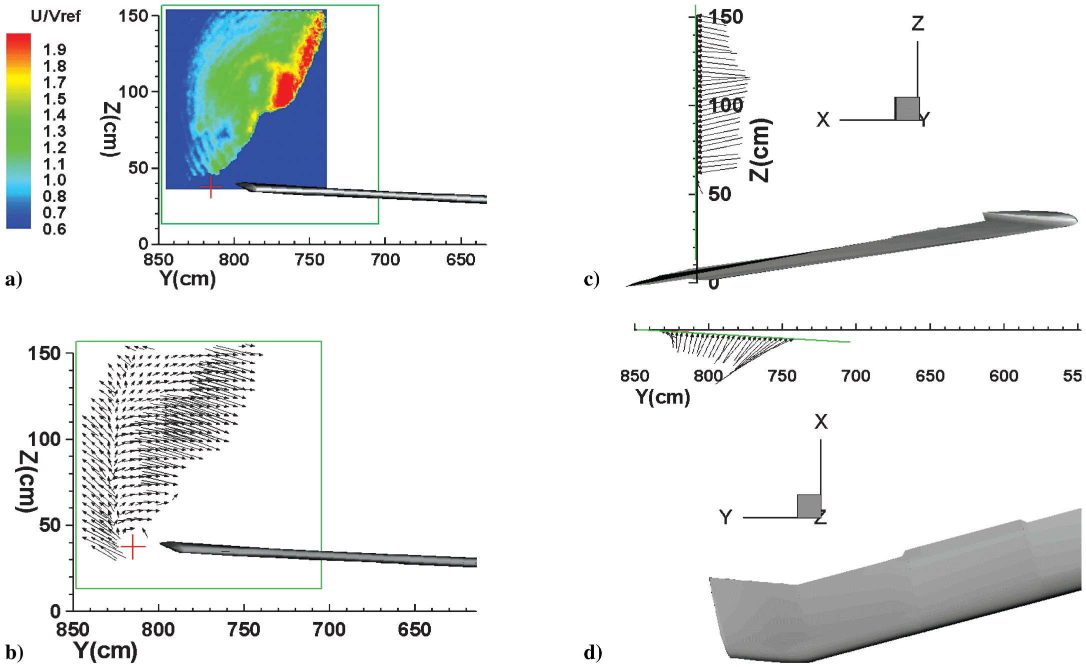

Fig. 12 Blade-wake velocity fields: axial velocity field contours and velocity vectors for $C_T = 0.06$.

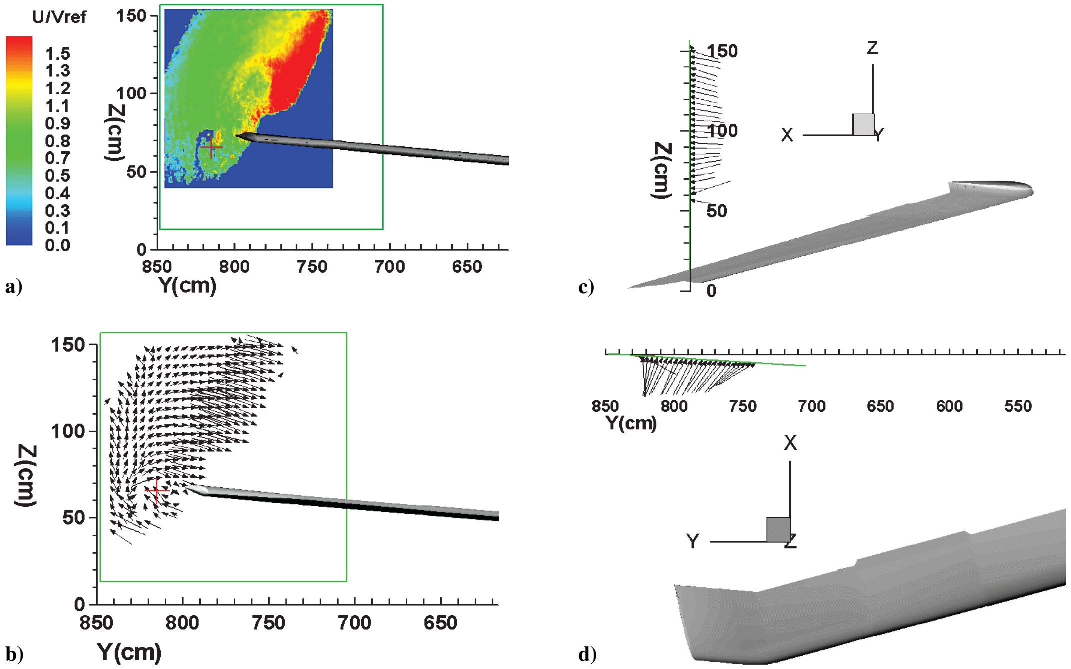

Fig. 13 Blade-wake velocity fields: axial velocity field contours and velocity vectors for $C_T = 0.10$.

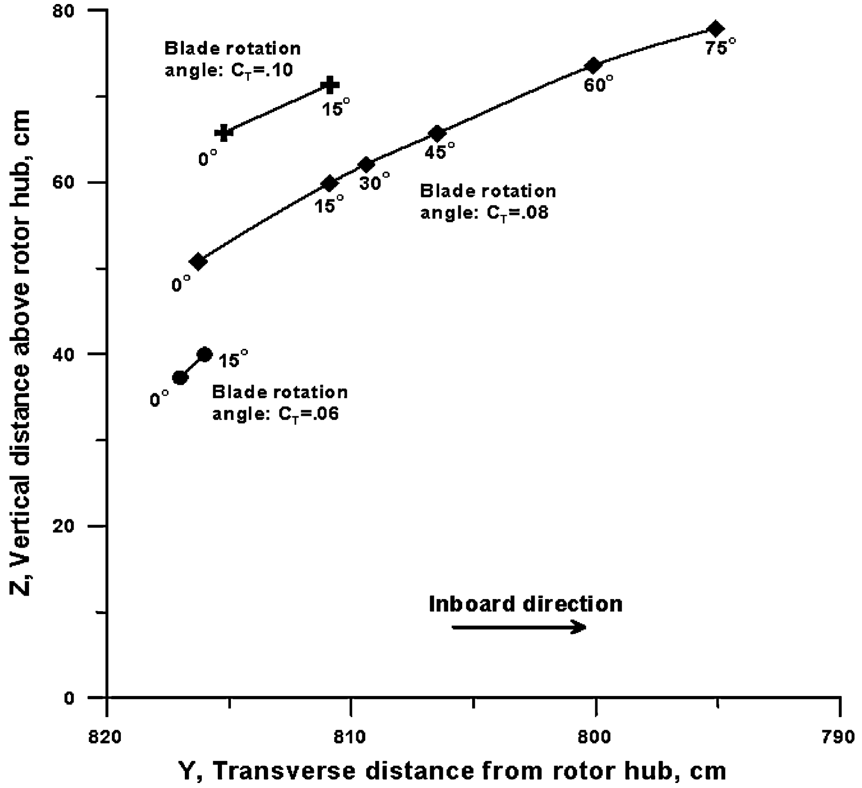

Fig. 14 Observed primary vortex core locations in *Y*, *Z* plane of light sheet for blade azimuth angles and thrust coefficients tested; blade azimuth angles measured in the upstream direction relative to plane of light sheet and indicated next to each data point; points marked 0 deg are at coordinates where blade passes through the light sheet.

Vortex core motion. A summary of the core center coordinates in the plane of the light sheet is shown in Fig. 14. Azimuth angles in the upstream direction relative the plane of the light sheet are indicated next to each data point. The 0-deg azimuth points for each thrust are the coordinates where the blade tip passes through the light sheet. All points represent observed core centers except for $C_T = 0.06$ and azimuth angle $= 15$ deg. That point was estimated from the vector field in Fig. 12b as described earlier. Figure 14 shows that as the blade azimuth increases, the location of the vortex core in the plane of the light sheet moves inboard. This movement is caused primarily by the geometric movement of downstream projection of the blade tip on the light-sheet plane as the blade rotates.

However, Fig. 14 also shows that the vortex is convected upward by the lifting flow over the rotor disk, which suggests that its inboard movement may also be influenced by the inboard circulation of the rotor disk flow. Finally, these results indicate that for a rotor with its rotation axis vertical, the vortex cores are always above the path of the next blade, and so there is no obvious opportunity for blade/vortex interaction in the plane of the light sheet on the advancing side of the rotor at these flight conditions.

Conclusions

These interblade wake measurements demonstrate the unprecedented capability of PDV to measure velocity vector field structures remotely in the dynamic wakes of a full-scale rotor operating in a large-scale facility. Similar measurements using other diagnostic methods are much less feasible at the ranges and flowfield sizes associated with this application. Other diagnostic methods that are based on the motion of optically resolved particles or aerosol structures must use high optical magnification and are accompanied by greatly reduced fields of view to image and track individual particles or clusters.

On the other hand, PDV measures the Doppler shift of scattered light from a cloud of aerosols and does not require the resolution of individual particles or clusters. By the use of standard 50-mm focal-length camera lenses, which give fields of view limited mainly by the entrance aperture of the split-image optics, these measurements demonstrate that the resulting spatial resolution is sufficient to locate and characterize the primary structures of rotor tip vortices and the general structure of the flow throughout the tip wake region. In other cases where the scale of the flow may be larger, the size of the features needed to characterize the flow should also increase, so that a wider field of view obtained over longer distances and with lower spatial resolution should still be sufficient to evaluate the flow geometry.

Single-pulse temporal resolution was not achieved in these tests because of the sporadic smoke distribution in the flow related to the in-draft tunnel inlet. To obtain images that filled the field of view, temporal averaging of several hundred image frames was required. However, single-pulse temporal resolution from uniform and steady aerosol seeding in a wind tunnel with recirculating flow would be much less difficult.

In general, these results demonstrate the performance of PDV in one of its most challenging applications and show that the PDV concept has been developed to the point were it can be used to obtain flowfield velocity vectors that describe the velocity field structure and magnitudes for large-scale, complex flows.

Acknowledgment

This work was performed by MetroLaser, Inc., under NASA Contract A55156D(NCV).

References

[1] McKenzie, R. L., and Reinath, M. S., "Planar Doppler Velocimetry Capabilities at Low Speeds and Its Application to a Full-Scale Rotor Flow," AIAA Paper 2000-2292, June 2000.

[2] McKenzie, R. L., "Measurement Capabilities of Planar Doppler Velocimetry Using Pulsed Lasers," *Applied Optics*, Vol. 35, No. 6, 1996, pp. 948–964.

[3] McKenzie, R. L., "Planar Doppler Velocimetry Performance in Low-Speed Flows," AIAA Paper 97-0498, Jan. 1997.

[4] Komine, H., Brosnan, S. J., Litton, A. B., and Stappaerts, E. A., "Real-Time, Doppler Global Velocimetry," AIAA Paper 91-0337, Jan. 1991.

[5]Meyers, J. F., “Doppler Global Velocimetry. The Next Generation?,” AIAA Paper 92-3897, Jan. 1992.

[6]Meyers, J. F., Lee, J. W., and Cavone, A. A., “Three Component Doppler Global Velocimeter Measurements of the Flow Above a Delta Wing,” Sixth International Symposium on Applications of Laser Techniques to Fluid Mechanics, July 1992.

[7]Lee, J. W., Meyers, J. F., Cavone, A. A., and Suzuki, K. E., “Doppler Global Velocimetry Measurements of the Vortical Flow Above an F/A-18,” AIAA Paper 93-0414, Jan. 1993.

[8]Elliott, G. S., Samimy, M., and Arnette, S. A., “A Molecular Based Velocimetry Technique For High Speed Flows,” *Experiments in Fluids*, Vol. 18, 1994, pp. 107–118.

[9]Clancy, P. S., and Samimy, M., “Multiple-Component Velocimetry in High Speed Flows Using Planar Doppler Velocimetry,” AIAA Paper 97-0497, Jan. 1997.

[10]Smith, M. W., Northam, G. B., and Drummond, J. P., “Application of Absorption Filter Planar Doppler Velocimetry to Sonic and Supersonic Jets,” *AIAA Journal*, Vol. 34, No. 3, 1996, pp. 434–441.

[11]Clancy, P. S., and Samimy, M., “Two-Component Planar Doppler Velocimetry in High-Speed Flows,” *AIAA Journal*, Vol. 35, No. 11, 1997, pp. 1729–1738.

[12]Reinath, M. S., “Doppler Global Velocimeter Development for the Large Wind Tunnels at Ames Research Center,” NASA TM 112210, Sept. 1997.

[13]Beutner, T. J., Elliott, G., Mosedale, A., and Carter, C., “Doppler Global Velocimetry Applications in Large Scale Facilities,” AIAA Paper 98-2608, June 1998.

[14]Mosedale, A. D., Elliott, G. S., Carter, C. D., Weaver, W. L., and Beutner, T. J., “On the Use of Planar Doppler Velocimetry,” AIAA Paper 98-2809, Jan. 1998.

[15]Smith, M. W., “The Reduction of Laser Speckle Noise in Planar Doppler Velocimetry Systems,” AIAA Paper 98-2607, June 1998.

[16]Meyers, J. F., Lee, J. W., Fletcher, M. T., and South, B. W., “Hardening Doppler Global Velocimetry Systems for Large Wind Tunnel Applications,” AIAA Paper 98-2606, June 1998.

[17]Beutner, T. J., Elliott, G., Williams, G. W., and Crafton, J., “Forebody and Leading Edge Vortex Measurements Using Planar Doppler Velocimetry,” AIAA Paper 2000-2294, June 2000.

[18]Elliott, G. S., and Beutner, T. J., “Molecular Filter Based Planar Doppler Velocimetry,” *Progress in Aerospace Sciences*, Vol. 35, 1999, pp. 799–845.

[19]Samimy, M., and Wernet, M. P., “Review of Planar Multiple-Component Velocimetry in High-Speed Flows,” *AIAA Journal*, Vol. 38, No. 4, 2000, pp. 553–574.

[20]Reinath, M. S., “Doppler Global Velocimeter Development for Large Wind Tunnels,” *Measurement Science and Technology*, Vol. 12, No. 4, 2001, pp. 432–441.

[21]Elliott, G. (ed.), “Special Feature: Molecular Filter Based Diagnostics,” *Measurement Science and Technology*, Vol. 12, No. 4, 2001, pp. 357–466.

[22]Forkey, J. N., “Development and Demonstration of Filtered Rayleigh Scattering—A Laser Based Flow Diagnostic for Planar Measurement of Velocity, Temperature and Pressure,” Ph.D. Dissertation 2067-T (TR 2067), Mechanical and Aerospace Engineering Dept., Princeton Univ., Princeton, NJ, April 1996, p. 177.

[23]Forkey, J. N., Finkelstein, N. D., Lempert, W. R., and Miles, R. B., “Demonstration and Characterization of Filtered Rayleigh Scattering for Planar Velocity Measurements,” *AIAA Journal*, Vol. 34, No. 3, 1996, pp. 442–448.

[24]Gerstenkorn, S., and Luc, P., “Atlas du Spectre d’ Absorption de la Molecule d’ Iode 14800–20000 cm^{-1},” Lab. AIME-COTTON, Centre National de la Recherche Scientifique, Orsay, France, 1978.

[25]McKenzie, R. L., “The Application of Planar Doppler Velocimetry to the Inter-Blade Wakes of a Full-Scale Rotor Flowfield,” NASA Contract A55156D(NCV), Final Rept., MetroLaser, Inc., Nov. 2001 (available from the author).

J. Trolinger
Guest Editor

Color reproductions courtesy of MetroLaser, Inc.